crystals

MDPI

Article

Microstructural, Corrosion and Mechanical Properties of Ni–Al–Cr/SiC Coatings on Inconel 600 Deposited by Arc Welding

Tayfun Çetin

Department of Electricity and Energy, Hakkari University, Hakkari 30000, Turkey; tayfuncetin@hakkari.edu.tr

Abstract

In this study, the microstructural, mechanical, wear, and corrosion behavior of Ni-Al-Cr and Ni–Al–Cr/SiC composite coatings with different composition ratios, produced by electric arc melting on Inconel 600 substrates, was systematically investigated. Microhardness measurements revealed a significant and consistent increase in the hardness values of the coatings depending on the increase in SiC reinforcement ratio (1%, 3%, and 5%). Wear tests showed that the coated samples exhibited significantly higher wear resistance compared to the pure Inconel 600 substrate. A significant improvement in wear resistance was achieved with the addition of SiC at 1% and 3% weight percentages; the width and depth of wear tracks were significantly reduced with SiC reinforcement. In contrast, increasing the SiC ratio to 5% weight percentage led to a decrease in wear resistance. This was attributed to particle aggregation at high SiC content, weakening of bonds at the matrix-reinforcement interface, and the behavior of SiC particles separated from the matrix as third-body abrasives. Electrochemical corrosion tests have shown that SiC-reinforced coatings form a more stable and permanent passive film, and corrosion resistance increases as the SiC content increases (1%, 3%, and 5%). The results indicate that the SiC reinforcement ratio affects the mechanical and electrochemical properties of Ni-Al-Cr/SiC composite coatings produced by electric arc melting.

Keywords: Inconel 600; arc welding; corrosion; wear; coatings; SiC; Ni-Al-Cr

1. Introduction

Inconel 600 is a nickel chromium iron alloy with an austenitic (FCC) structure, having a nominal of Ni–16Cr–9Fe, and is characterized by its good corrosion and oxidation resistance at high temperatures. The high nickel content provides resistance to corrosion in organic and inorganic solutions, while the high chromium content provides resistance to sulfur compounds and oxidizing conditions at high temperatures [1–3]. Such properties enable Inconel 600 to be one of the most widely used nickel-based alloys in high temperature applications such as heat exchangers of power plants, heat treating furnaces, as well as turbine engine parts in aerospace, chemical, and marine industries [1–4]. Despite good corrosion resistance, Inconel alloys are susceptible to intergranular corrosion (IGC) owing to carbide precipitation at grain boundaries in addition to inadequate wear performance [5]. Therefore, to increase the long-term durability of Inconel alloys, surface modification and protective coating treatments are essential. To enhance the surface properties of Inconel 600, Various surface modification and coating methods such as diffusion boriding, nitriding, laser coating, gas tungsten arc welding, plasma sputtering, high velocity oxygen fuel (HVOF) sputtering, physical vapor deposition (PVD), plasma assisted chemical vapor

Check for updates

Academic Editor: Shouxun Ji

Received: 17 December 2025
Revised: 5 January 2026
Accepted: 7 January 2026
Published: 11 January 2026

deposition (PACVD), and arc melting have been investigated in the literature for Inconel 600 [4,6–8]. While each of these methods offers different advantages, criteria such as coating substrate bond strength, coating thickness, and production cost are important parameters determining the choice of method. Due to its high bond strength and relatively low cost, electric arc melting technique has emerged as a noteworthy alternative in recent years [9].

It has been reported that coatings obtained by arc melting significantly increase the surface hardness and wear resistance in alloys containing Ni or Fe. Ning et al. (2023) [10] investigated the microstructure, hardness, residual stress, and wear properties by producing composite coatings reinforced with SiC at different fractions on Inconel 718 by laser cladding (LC). Wear resistance increased significantly as the SiC fraction increased. Makuch et al. (2023) [11] applied laser surface alloying with WC particles to increase the wear resistance of Inconel 600. Coatings containing WC showed significantly higher wear resistance than uncoated Inconel 600. Kulka et al. (2013) [4] obtained a thick and hard layer consisting of Ni_2B, Ni_3B, CrB, Cr_2B, Fe_3B and Ni–Cr–Fe phases on the surface of Inconel 600 by laser boronizing method and stated that this method is more efficient than diffusion boronizing. Ghadami et al. (2015) [12] applied WC–Co coating to steel surfaces using the air plasma spray (APS) method and then melted the surface using TIG. The melted coatings showed lower wear rates than the sputtered coatings. Xie et al. (2006) [13] reported that the SiC reinforcement increased surface hardness and wear resistance by laser on a Ni60–SiC/Ti_3SiC_2 composite coating onto IN718. Wang et al. (2025) [14] produced Inconel 625 composites reinforced with nanosized WC at different ratios (0%, 2%, 6% and 10%) using circular oscillating laser direct energy deposition (LDED) method. WC reinforcement led to significant improvements in microhardness and wear resistance. Sitek et al. (2008) [7] produced multilayer coatings consisting of σAl_2O_3 + Ni_3Al + Ni(Cr,Fe,Al) + Cr_7C_3 + Cr-Ni phases on Inconel 600 via plasma-enhanced chemical vapor deposition (PACVD), achieving a surface hardness of 1200 HV alongside high heat and abrasion resistance. Calderón et al. (2014 [15] investigated the erosion corrosion behavior of Ni-based composite coatings reinforced with SiC nanoparticles. They determined that the addition of SiC to electrochemically produced coatings led to grain refinement and changes in coating morphology. The results showed that SiC nanoparticles increased coating hardness and significantly improved erosion-corrosion resistance compared to pure nickel coatings. Medelien (2002) [16] investigated the formation of Ni–SiC and Ni–B_4C composite coatings with pure nickel plating. Ni–SiC composite coatings showed the formation of a dense and stable structure and high fracture resistance. Maurya et al. (2024) [17] conducted a study on the effect of pulse frequency on the microstructure, mechanical properties, and corrosion resistance of Ni-SiC composite coatings produced by electroplating. They reported that in SiC/Ni composite coatings produced by pulse electrodeposition, a more homogeneous structure and higher SiC content were obtained at low frequencies (especially 10 Hz); this reduced electrolyte penetration, suppressed local corrosion, and provided high corrosion resistance with a lower corrosion rate compared to pure Ni coatings. Hou et al. (2025) [18] investigated the corrosion and wear behavior of Ni/SiC composite coatings produced by electrodeposition method under different environmental conditions. The study showed that the addition of SiC refined the Ni grain structure, increased hardness, and improved surface integrity. The authors reported that Ni/SiC coatings offered superior tribocorrosion resistance under complex service conditions.

In this study, Ni–Al–Cr/SiC composite coatings, prepared in specific proportions, were fabricated on the surface of Inconel 600 alloy via the electric arc melting method. Differences in thermal expansion coefficient and metallurgical compatibility between the coating material and the substrate can cause tensile stresses in the coating layer and, as a result, the development of defects such as cracking, peeling, or delamination. Therefore, it is

https://doi.org/10.3390/cryst16010049

crucial that the matrix and reinforcement phases selected in coating systems exhibit thermal and metallurgical properties compatible with the substrate material. In this context, it is aimed to achieve high bond strength, oxidation resistance, and metallurgical compatibility in the coating layer by using Ni-Al-Cr matrix powders and SiC particles. During the coating, a Ni–Cu based Monel 400 electrode was used to ensure metallurgical compatibility between the Inconel 600 substrate and the Ni–Al–Cr/SiC layer. Monel exhibits high chemical compatibility with nickel-based alloys and, thanks to its coefficient of thermal expansion close to Inconel 600, reduces residual stresses that may occur during cooling. It also acts as an interlayer, ensuring strong bonding of the coating layer to the substrate surface and preventing crack formation. The resulting coatings were microstructurally characterized using SEM/EDS and XRD analyses. Wear resistance, hardness distribution, and electrochemical corrosion tests were also conducted. The results showed that the Ni–Al–Cr/SiC coatings produced by arc melting significantly improved the surface properties of Inconel 600.

2. Materials and Methods

2.1. Material

Inconel 600 alloy and Ni, Al, Cr, and SiC powders with 99+% purity and 325 mesh size were commercially supplied by Nanografi Co., Ankara, Turkey. Five Inconel 600 specimens were prepared with dimensions of 100 × 40 mm^2 in a rectangular shape for experimental studies. The cutting process was carried out using a Metkon Micracut 202 abrasive cutter (Metkon Instruments Inc., Bursa, Turkey) to ensure dimensional precision, and any surface roughness or deformations induced by the cutting process were eliminated by mechanical grinding. Monel electrodes were used in the coating process due to their balanced alloy composition and high adaptability to welding conditions. The chemical composition of Inconel 600 is given in Table 1, and the chemical composition of the Monel 400 electrode is given in Table 2.

Table 1. Inconel 600 alloy chemical composition.

Ni (wt.%)	Cr (wt.%)	Fe (wt.%)	C (wt.%)	Mn (wt.%)	S (wt.%)	Si (wt.%)	Cu (wt.%)
72.9	16.1	8.4	0.3	0.1	0.015	0.001	0.5

Table 2. Chemical composition of Monel 400 electrode.

Ni (wt.%)	Cu (wt.%)	Fe (wt.%)	Mn (wt.%)	Si (wt.%)	C (wt.%)	S (wt.%)
63.2	29.3	2.1	1.5	0.3	0.2	0.01

2.2. Electric Arc Melting Procedure

V-shaped grooves 5 mm deep and 5 mm wide were made on the upper surfaces of the samples. The Ni–Al–Cr/SiC powder mixture was mixed in a Turbula mixer (Ikiler Instruments Inc, Istanbul, Turkey) for 12 h to ensure homogeneous distribution, then placed in the grooves and compacted under 100 MPa pressure. In the coating system, the Ni-Al-Cr alloy was used to ensure metallurgical compatibility with the substrate material, increase adhesion strength, and improve oxidation resistance. SiC particles, which are brittle on their own, were bound by the Ni-Al-Cr matrix phase, supporting the ductility and structural integrity of the coating. In addition, ensuring the thermal expansion and chemical compatibility of the powder components with the Inconel substrate is critical to preventing cracks and separations at the interface. Accordingly, preliminary trials were carried out at different composition ratios, and the most suitable powder composition was selected based on the results obtained and applied to the coating process.

https://doi.org/10.3390/cryst16010049

Arc welding was performed using an Askaynak Inverter 205 welding machine (Askaynak Welding and Cutting Technologies, Istanbul, Turkey) with 90 A DC electrode positive polarization (DCEP) at the 1G position. The electrode angle was 45°, the travel speed was 12 cm/min; the welding arc length was 3.25 mm and the electrode diameter was Ø3.25 mm. These parameters were optimized as a result of preliminary trials. The proportions of Ni, Al, Cr, and SiC used in the coating and their sample codes are given in Table 3.

Table 3. Coating composition and SiC fractions.

Sample Code	Compound	Total Weight (g)	SiC Fraction (%)
S1	Inconel	-	-
S2	Ni–Al–Cr	50 (44 + 2 + 4)	0% SiC
S3	Ni-Al-Cr + SiC	50 + 0.5 = 50.5	1% SiC
S4	Ni-Al-Cr + SiC	50 + 1.5 = 51.5	3% SiC
S5	Ni-Al-Cr + SiC	50 + 2.5 = 52.5	5% SiC

2.3. Microstructure Analysis

The coated samples were subjected to abrasive grinding using 200, 400, 600, 800, 1000 and 1200 grids, respectively. The surface ground samples were polished with 6 and 3 µm felts. The samples were then etched with HNO_3 and H_2SO_4 etchant at a 1:1 ratio and were ready for micro examination. Microstructure images of the samples were taken at high resolution with a field emission scanning electron microscope (FESEM, Zeiss Sigma 300 (Carl Zeiss Microscopy GmbH, Oberkochen, Germany)). FESEM analysis was performed using a ZEISS Sigma 300 instrument)), at an acceleration voltage of 10 kV (EHT) and with a secondary electron (SE2) detector. Elemental mapping and point analyses were carried out using the Energy Dispersive X-Ray Spectroscopy (EDS) method with the SE2 detector at an accelerating voltage of 20 kV. The crystal structure of the samples was determined using Rigaku Ultima-IV X-ray diffractometer (XRD) (Rigaku Corporation, Tokyo, Japan) operating under Cu Kα (λ = 1.5406 Å) radiation, 30 mA current and 40 kV voltage conditions.

2.4. Mechanical Tests

Microhardness and wear tests were carried out to determine the mechanical properties of the samples. The surfaces of the samples were polished before hardness testing. Microhardness measurements were performed using the Vickers method with a Bulut Makina Microbul 1000-AT-PC device (BMS Bulut Makina Industry and Trade Ltd. Co., Kocaeli, Turkey). Measurements were carried out under a load of 0.5 kgf ($HV_{0.5}$) for 12 s, and hardness values were recorded at 11 distinct points on each sample, ranging from the coating point to the Inconel 600 surface. To investigate the wear behavior, dry sliding wear tests (ball-on-disk) were applied with a UTS Tribometer (UTS Scientific Instruments, Trabzon, Turkey) testing device. An AISI 52100 stainless steel ball was used as the counter surface in the experiments. During the tests, three different loads (20 N, 30 N and 40 N) were applied, and the stroke distance was set as 7 mm and the total sliding distance was 250 m. A back-and-forth sliding motion was applied during wear test.

2.5. Electrochemical Corrosion Test

Electrochemical corrosion tests were carried out using a PalmSens EmStat4R potentiostat (PalmSens BV, Houten, The Netherlands) according to ASTM G59 [19]. The experiments were conducted in a conventional three-electrode electrochemical cell, where the specimens served as the working electrode, an Ag/AgCl electrode was employed as the reference, and a platinum wire functioned as the counter electrode. The electrolyte medium consisted of an aqueous 3.5 wt.% NaCl solution for harsh conditions simulations. Firstly, the specimens were mounted in a cold resin, leaving an effective exposed area of 2 cm^2. Before polarization measurements, the open circuit potential (OCP) of each sample was monitored for 2400 s to allow stabilization of the electrochemical cell. After reaching a steady-state potential, potentiodynamic polarization (PDP) tests were performed by scanning the potential from −0.6 V relative to the E_{OCP} toward the cathodic direction with −1.2 V relative to E_{OCP} at anodic slope, at a sweeper rate of 1 mV/s. In addition, electrochemical impedance spectroscopy (EIS) was employed to analyze the corrosion behavior and oxide film formation characteristics of the samples. EIS measurements were conducted after completion of the polarization tests, applying a sinusoidal perturbation of 10 mV around the OCP over a frequency range spanning from 100 kHz to 0.01 Hz. The obtained impedance spectra were analyzed using EC-Lab software (v10.40, Demo version). To verify experimental consistency, all electrochemical tests were repeated three times, yielding highly reproducible results.

3. Results and Discussion

3.1. Morphological and Structural Results

The microstructural properties of the samples were investigated by scanning electron microscopy (SEM), X-ray diffraction (XRD), and energy dispersive spectroscopy (EDS) analyses to evaluate the morphology, grain structure, surface integrity, and phase composition of the coating layer.

The SEM images in Figure 1a,b show the microstructural transition between the Inconel substrate and the weld zone. A distinct resolidification structure has formed in the weld zone, with dendritic and cellular solidification morphologies concentrated in different regions depending on the heat input. The heat-affected zone (HAZ) extends towards the weld zone with typical thermal effects such as grain coarsening, precipitation dissolution, and redistribution.

SiC particles dispersed throughout the coating are trapped within the matrix during welding and maintained as a separate phase in the microstructure (Figure 1c–h). These particles influence solidification in the weld zone, contributing to the formation of a finer and more oriented dendritic structure. Due to the difference in high melting point and thermal conductivity, SiC is insoluble in the weld pool and disperses within the matrix as a hard, stable reinforcement phase [20]. In the heat-treated zone, a distinct thermal transition zone forms between the Inconel matrix and the weld metal; slight grain boundary separation and oriented grain growth are observed. Dendritic structure density increases towards the weld zone, leading to rapid solidification conditions. SiC reinforcement ensures more homogeneous and oriented microstructure in the weld zone, maintaining structural continuity between the Inconel substrate and the weld metal, and allowing for a more homogeneous distribution of particles within the matrix. SEM images reveal that as SiC content increases, there are more particles at the grain boundaries, and these particles limit the regular growth of the dendritic structure. Particularly in samples with 3% and 5% SiC content, a denser interdendritic SiC phase was observed. Microhardness and wear measurements show parallelism with SEM observations, and 3% SiC content is considered the limiting value for wear testing [21,22].

The mean values of main elements in Inconel alloys were observed using EDS element mapping analysis. The dominant element of the alloy (42 wt.%) is Ni and is distributed homogeneously throughout the matrix. The uniform distribution of Cr (28 wt.%) and Fe (25 wt.%) confirms that the chemical continuity inherent in the Inconel structure is maintained. The low density but uniform distribution of minor elements such as Si (3 wt.%) and Al (2 wt.%) supports the microstructural integrity of the alloy. These results demonstrate that the studied region has a chemically stable and uniform phase structure. The line scan EDX analysis was carried out for weld zone, HAZ, and Inconel alloy to monitor elemental changes in Figure 2. It is clear that the concentration of Si is slightly reduced at the HAZ and Inconel zone.

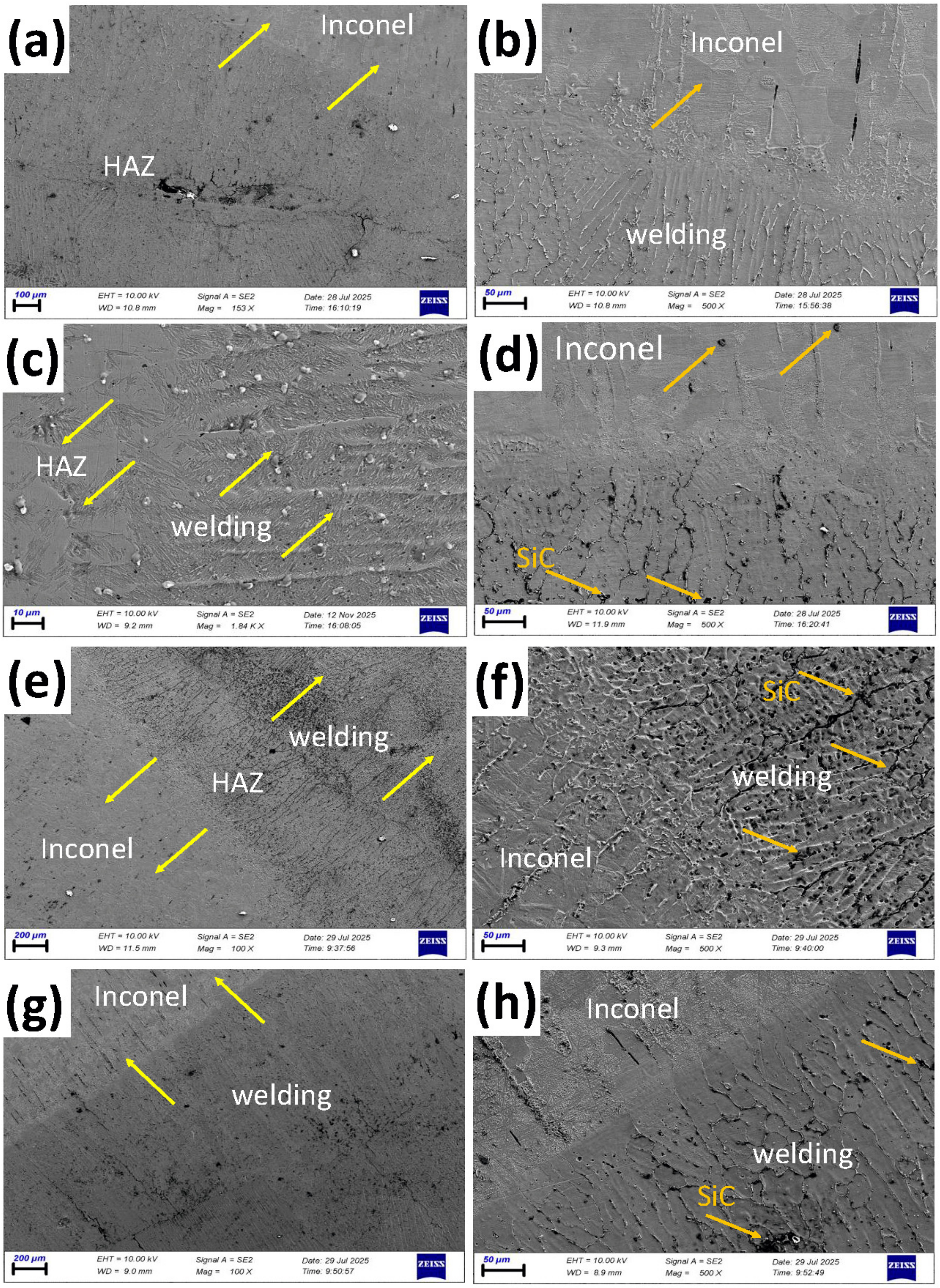

Figure 1. SEM Microstructure Images of Inconel 600/Weld Zone and SiC-Reinforced Samples: (**a**,**b**) S2, (**c**,**d**) S3, (**e**,**f**) S4, (**g**,**h**) S5.

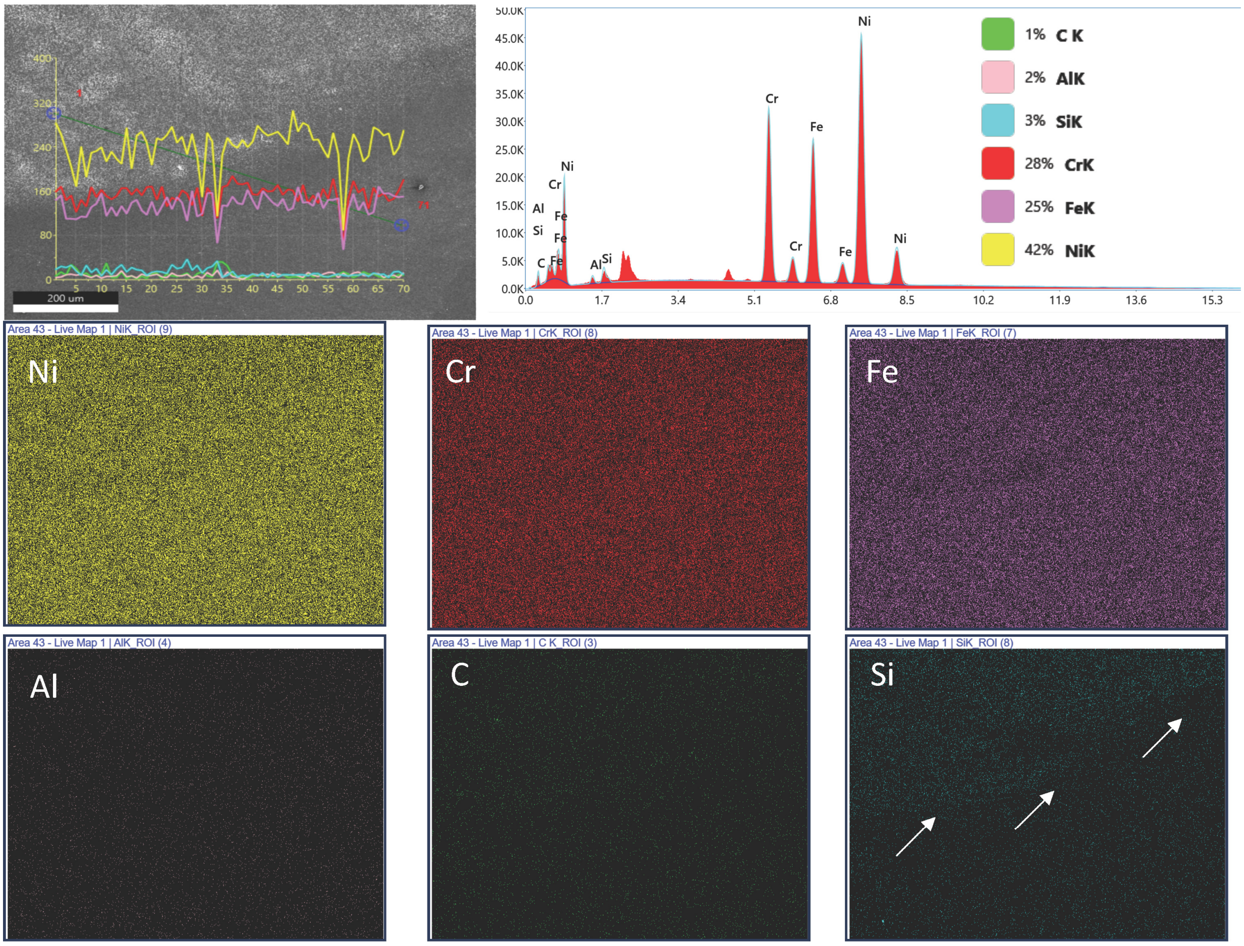

Figure 2. Line EDS mapping (from welding to base metal).

The crystal structure of coating materials was determined using XRD analysis peaks in Figure 3. The characteristic peaks of the Ni-Al-Cr matrix (111), (113), (200), and (300) planes were clearly observed in all samples, indicating that the matrix phase maintained its dominance throughout the coating. The characteristic peaks that appeared at $2\theta = 75^{\circ}$ are assigned to SiC (0008) [23]. To describe the orientations of planes symmetrically and equivalently in the hexagonal crystal structure of SiC, the Miller–Bravais four-digit (hkil) indexing system is used. The classical three-digit (hkl) index cannot explicitly represent this type of symmetry, and therefore the four-digit notation is preferred in hexagonal systems. Additionally, the (113) peak appeared at $2\theta = 43^{\circ}$, representing the main crystal planes of $NiCr_2O_4$ intermetallic phases. The formation of this phase can be associated with oxidation processes occurring during or after coating and is reported in the literature. Liang et al. (2011) [24] investigated the oxidation behavior of NiCoCrAlY coatings and reported the formation of the $NiCr_2O_4$ spinel phase on the Cr_2O_3 layer during high-temperature oxidation. Gray et al. (2024) [25] compared the oxidation behavior of the $NiCr_2O_4$ and Cr_2O_3 phases and reported that the $NiCr_2O_4$ spinel phase forms a more stable oxide layer under certain conditions. The observation of characteristic peaks belonging to the Inconel substrate material, albeit at low intensity, in some samples indicates that the coating thickness is sufficient to allow partial penetration of X-rays into the substrate. Overall, XRD results indicate that the reinforcement of SiC does not lead to the formation of new phases in the coating but rather increases the density of existing phases and the detectability of the ceramic phase. Furthermore, SiC supports the multiphase structure of the composite coating and contributes to its structural stability.

https://doi.org/10.3390/cryst16010049

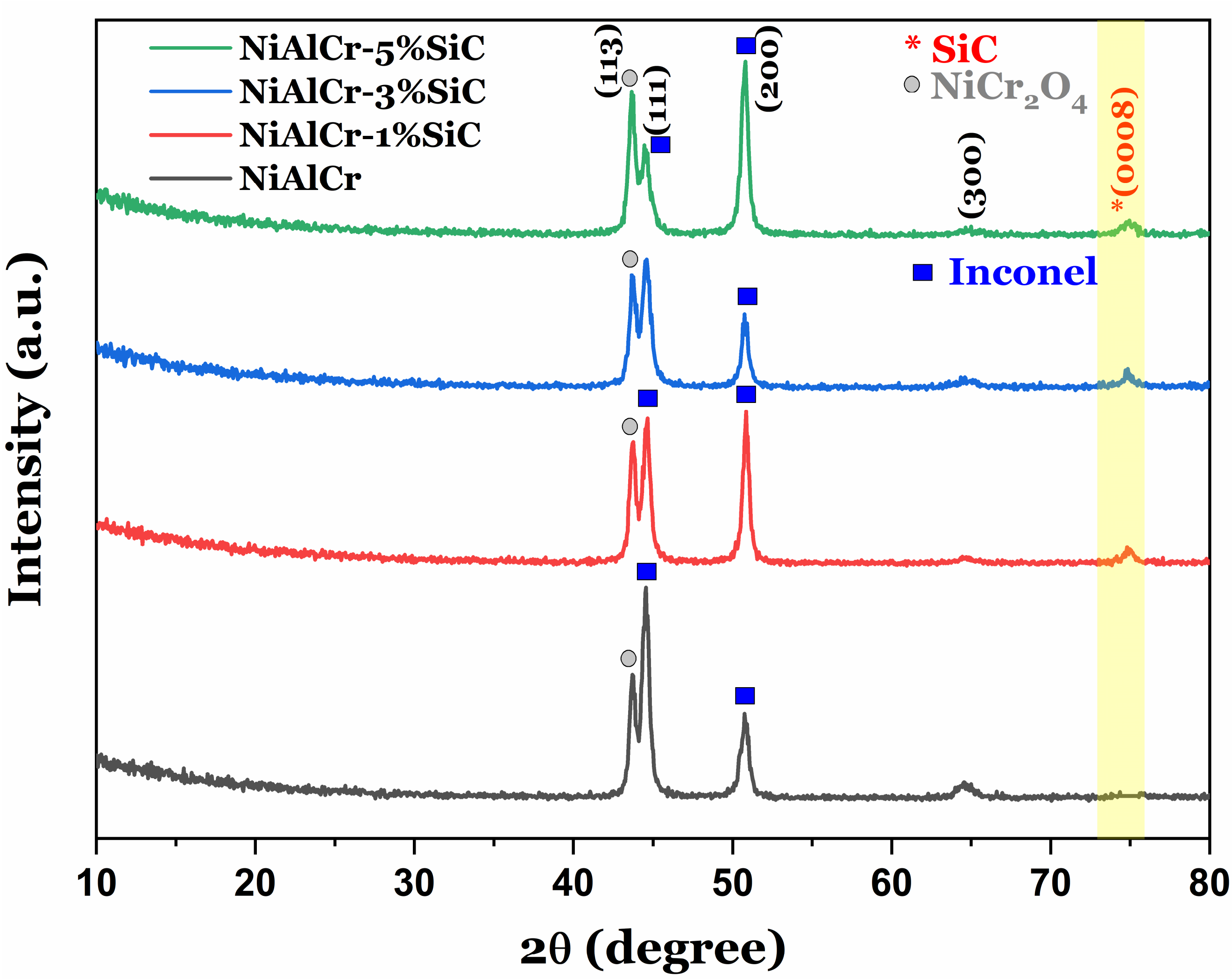

Figure 3. XRD Patterns of NiAlCr Coatings with Different SiC Reinforcement Fractions.

3.2. Microhardness Results

Microhardness measurements were carried out to evaluate the surface mechanical properties of the samples. It is observed that the reinforcement of SiC at different rates to the Ni-Al-Cr matrix has a significant effect on the coating hardness (Figure 4). As the SiC fraction increases, microhardness values in the coating region increase significantly. In particular, the Ni–Al–Cr/5%SiC coating exhibits the highest hardness compared to the other compositions, reaching approximately 390 $HV_{0.5}$ in the region closest to the surface. This can be interpreted as the SiC reinforcement promotes the formation of high-hardness ceramic phases in the coating structure and increases hardness by limiting dislocation motion. Furthermore, the porosity observed during coating is attributed to the incomplete dissolution of the SiC powder differences in particle sizes [26]. Hardness values are observed to decrease rapidly in measurements taken 2 mm from the surface. This decrease can be explained by the crossing of the coating layer boundary and the arrival of the substrate region. Due to the lower hardness of the substrate, microhardness values drop to approximately 150 $HV_{0.5}$. This transition region is important for assessing the quality of the bond between the coating and the substrate and the continuity of the transition.

https://doi.org/10.3390/cryst16010049

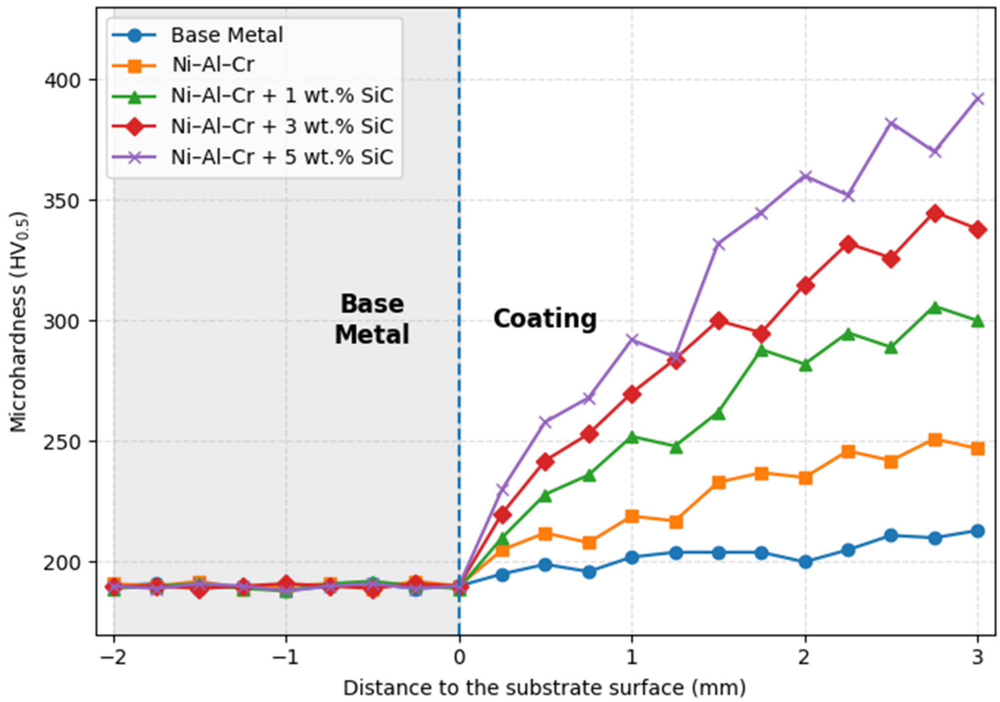

Figure 4. Effect of Different SiC Reinforcement Fractions on Microhardness Distribution in the Coating Region.

3.3. Wear Test Results

Wear tests are critical for understanding how the mechanical strength of the coating and the surface change under tribological conditions. Figure 5 shows the results of the wear test. Especially in Inconel-based super-alloys operating under high temperatures and friction conditions, the wear behavior of surface coatings directly affects the service life of the material. Therefore, examining the contribution of SiC reinforcement to the wear resistance of Ni-Al-Cr coatings provides important insights into both mechanical strengthening and surface protection. As can be seen in Figure 5, the highest wear rate was measured in the Inconel 600 base material (~0.35 × 10^{-3} mm^3/Nm). Ni-Al-Cr coating (S2) significantly reduced the wear rate compared to Inconel 600. This improvement can be attributed to the Cr element increasing the oxidation resistance and strengthening the load-carrying capacity of the coating [27]. The reinforcement of 1% and 3% SiC to the coating provided the most significant reduction in wear rate. This can be explained by the dispersion of the particles as the load-carrying phase in the matrix and the inhibition of dislocation movement [28]. The wear rate tended to increase in the coating containing 5% SiC. This was attributed to the fact that the high SiC content embrittled the coating, leading to microcracks. The results show that the experimental findings are consistent with the literature. SiC reinforcement reduces wear rates by increasing hardness; however, excessive SiC reinforcement reduces coating ductility and leads to brittle behavior. The maximum SiC content is approximately 3%, and this composition exhibit the best balance of performance between high hardness and low wear.

Following wear tests, the wear surfaces of the samples were examined in detail using scanning electron microscopy. The SEM images obtained after wear are shown in Figure 6, revealing the changes in the surface morphology of the samples and the wear mechanisms. The large plastic deformation regions, prominent adhesive tears, and discontinuous tribo oxide layers observed in the SEM images of the pure Inconel surface (Figure 6a,b) are associated with the susceptibility of nickel-based superalloys to adhesive wear due to their relatively low surface hardness and high ductility, leading to strong metal-to-metal contact with the mating surface [29]. In the literature, it has been reported that oxide films formed during friction, especially when unstable, enter a fracture reformation cycle, failing to adequately protect the surface and accelerating material loss [30,31]. Similar adhesive wear morphologies and discontinuous tribo oxide layers have been widely reported in numerous studies for Ni-based alloys [32,33]. In the SEM images of the Ni-Al-Cr coated samples (Figure 6c,d), it is seen that the wear track is significantly narrowed, the plastic deformation on the surface is reduced, and a more stable and continuous oxide layer is maintained throughout the coating. This situation can be explained by the fact that in Ni-Al-Cr based coatings, Al and Cr elements increase surface integrity and limit metal–metal contact by forming thermodynamically stable oxides such as Al_2O_3 and Cr_2O_3 during friction. In the study by Yu and Tang (2022) [27], it was similarly reported that stable and compact oxide layers act as a load-bearing tribo layer on the surface, thereby suppressing the tendency for adhesive wear. In the SEM images of the 1% SiC-reinforced coating (Figure 6e,f), it is observed that the wear track has a more homogeneous character, local material accumulations on the surface are reduced, and abrasive microcut marks are significantly softened. This improvement can be attributed to the SiC particles acting as a hard and stable load-bearing phase within the matrix and increasing the mechanical stability of the coating surface by limiting dislocation movement [34].

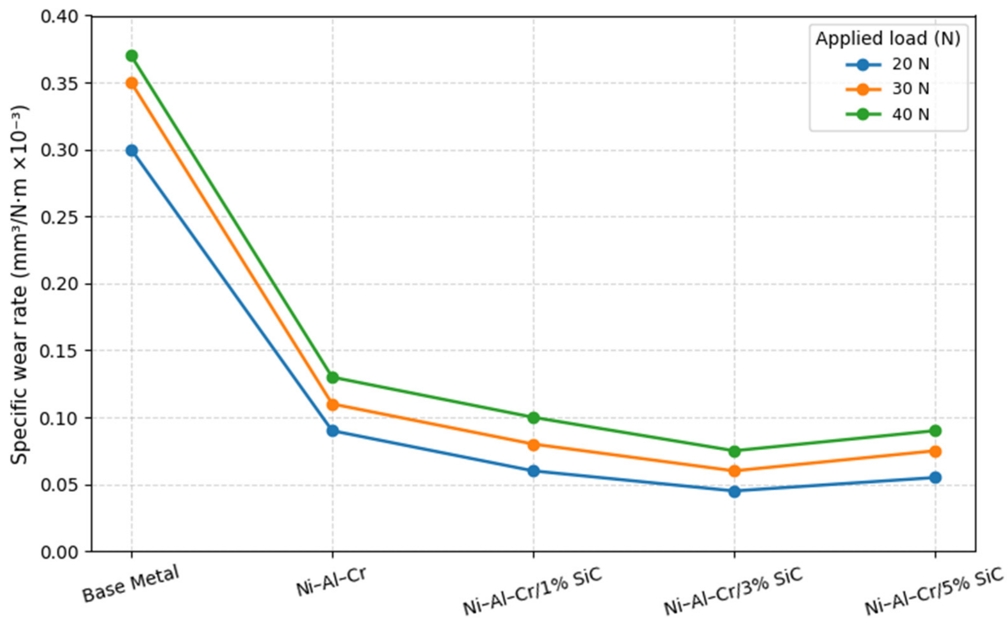

Figure 5. Wear Rate Comparison of Inconel 600 and Ni–Al–Cr/SiC Coatings under Different Loads.

In samples where the SiC fraction is increased to 3% (Figure 6g,h), it is observed that the wear zone becomes finer and more regular, microfractures are largely suppressed, and a more continuous deformation structure develops throughout the coating. This shows that the particle distribution maintains its homogeneity and the hard reinforcement phase effectively distributes the tribological load [35].

In a comprehensive study on Inconel 718/SiC composite coatings by Ning et al. (2023) [10], it was reported that with increasing SiC content, the width and depth of wear tracks decreased up to 7% weight, but at 10% SiC level, the wear tracks widened again and the surface morphology became irregular. SEM images reveal that adhesive wear is partially suppressed with Ni-Al-Cr coating, abrasive wear mechanisms are controlled with SiC reinforcement, and optimum tribological performance is achieved at medium SiC content (S4).

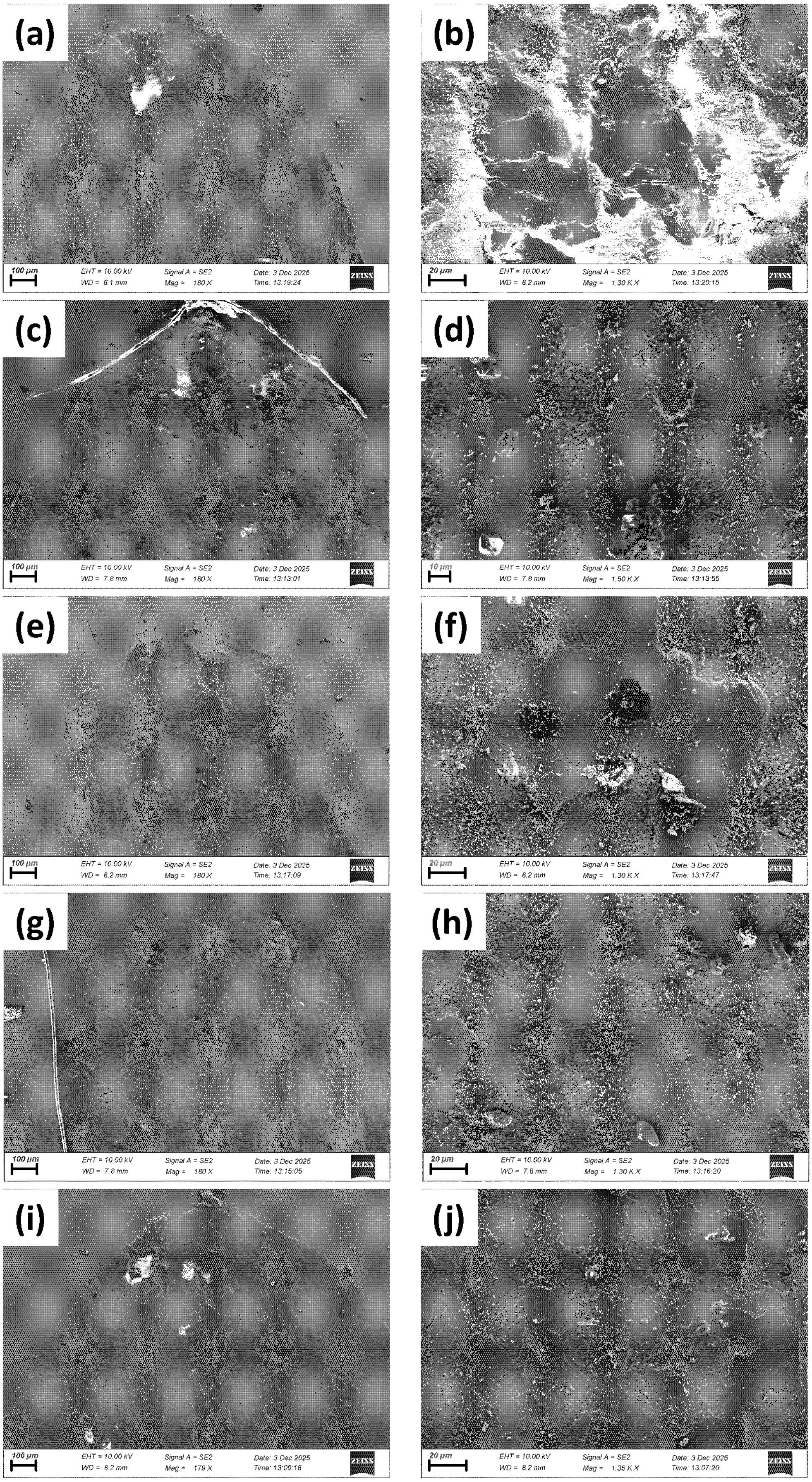

Figure 6. SEM images of samples after wear testing: (**a**,**b**) S1, (**c**,**d**) S2, (**e**,**f**) S3, (**g**,**h**) S4, and (**i**,**j**) S5.

3.4. Electrochemical Corrosion Test Results

Figure 7a shows the time-dependent open circuit potential (OCP) curves. While the potential of uncoated Inconel 600 remains stable at approximately −0.35 V, the potential shifts to more positive values in Ni-Al-Cr and SiC-doped coatings. This indicates that the passive oxide layer formed on the surface increases electrochemical stability. Garcia et al. (2003) [36] reported that the positive potential shift in Ni-SiC coatings is related to passive film integrity. Figure 7b shows the Tafel curves, revealing that the uncoated surface has the highest corrosion current density ($\boldsymbol{I_{corr}}$). With the Ni-Al-Cr coating, $\boldsymbol{I_{corr}}$ decreased by approximately half, and this decrease became more pronounced with the reinforcement of SiC. It is observed that, especially in the sample with 5 wt.% SiC (S5), both $\boldsymbol{I_{corr}}$ decreased to a minimum and the corrosion potential ($\boldsymbol{E_{corr}}$) reached the most positive value. This can be explained by the homogeneous distribution of SiC particles, increasing the coating density and restricting the ion diffusion paths. Nyquist diagrams are given in Figure 7c. The magnitude of the circle radius represents the charge transfer resistance (Rct ≈ R_3). While the smallest radius was observed on the uncoated surface, the radius increased with the SiC content and reached a maximum in the sample with 5 wt.% SiC (S5). As a result, examined in Figure 7a–c, it is shown that SiC addition significantly improves the electrochemical stability of Ni-Al-Cr coatings.

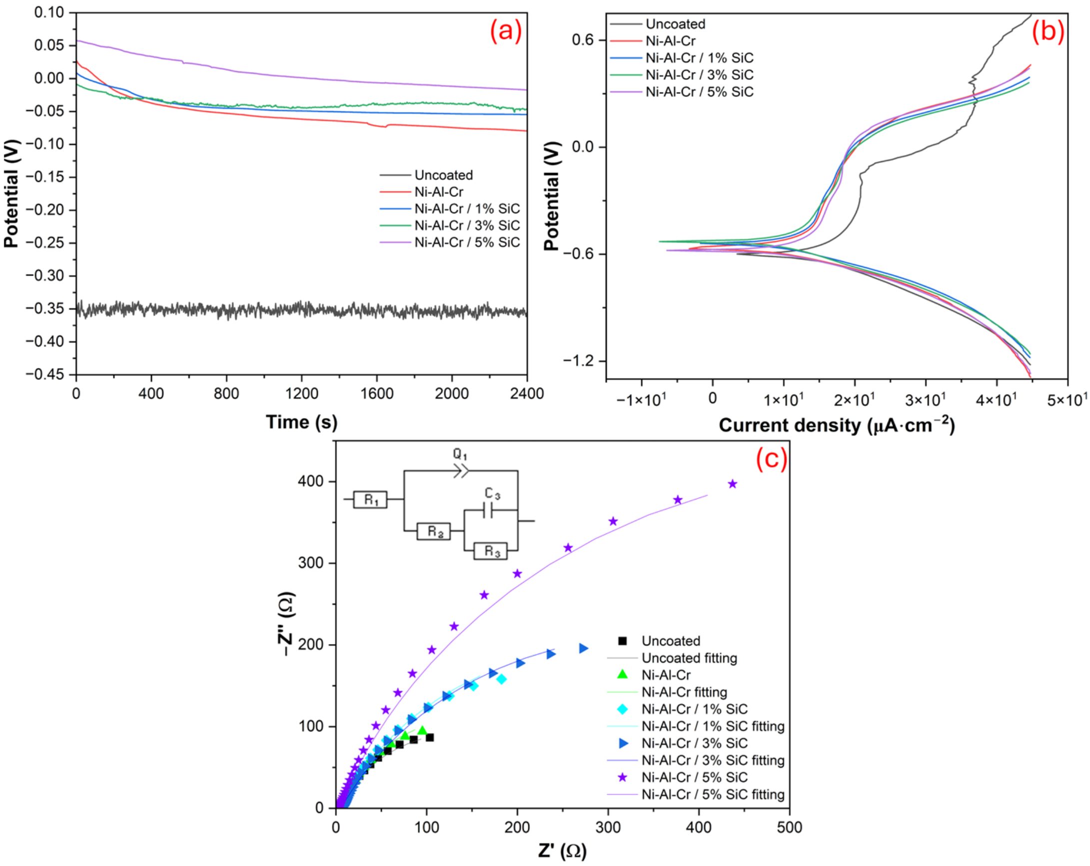

Figure 7. Electrochemical corrosion behavior of Inconel 600 and Ni–Al–Cr–SiC coatings in 3.5 wt.% NaCl solution; (**a**) OCP, (**b**) PDP, and (**c**) EIS results.

Coatings were investigated using the potentiodynamic polarization (PDP) test. Corrosion potential ($\boldsymbol{E_{corr}}$), corrosion current density ($\boldsymbol{I_{corr}}$), anode and cathode slope coefficients ($\boldsymbol{\beta_a}$ and $\boldsymbol{\beta_c}$), and polarization resistance ($\boldsymbol{R_p}$) were calculated from the obtained Tafel curves, and the results are given in Table 4.

Table 4. Tafel extrapolation data obtained from PDP curves.

Sample	E_{corr} (V)	I_{corr} (mA/cm^2)	β_a (V/Decade)	β_c (V/Decade)	R_p (Ω)	*Corrosion Rate* (mm/Year)
Uncoated (S1)	−0.598	12.0	0.44	0.18	1840	0.127
Ni-Al-Cr (S2)	−0.568	6.2	0.68	0.14	3303	0.066
Ni-Al-Cr/1%SiC (S3)	−0.538	5.8	0.67	0.13	3368	0.062
Ni-Al-Cr/3%SiC (S4)	−0.528	5.2	0.54	0.15	3916	0.055
Ni-Al-Cr/5%SiC (S5)	−0.578	5.1	0.61	0.13	3624	0.055

It is seen that the uncoated Inconel 600 sample has the highest corrosion current density (I_{corr} = 12 μA/cm^2) and the lowest polarization resistance (R_p = 1840 Ω) (Table 4). This indicates that the passive film formation on the bare surface is weak and the metal interacts directly with the electrolyte. With the application of the Ni-Al-Cr coating, the Icorr value decreased to 6.2 μA/cm^2, and the R_p value increased to 3303 Ω. This improvement indicates that the coating forms a more stable oxide layer on the surface and reduces the corrosion rate by limiting ion transport. This trend became even more pronounced with increasing SiC reinforcement. In particular, the coating containing 5 wt.% SiC demonstrated optimum corrosion resistance by reaching the lowest I_{corr} (5.1 μA/cm^2) and the highest R_p (3624 Ω) values. This proves that SiC particles increase the density of the coating structure, reduce porosity, and thus strengthen the passive film integrity. Therefore, the optimum SiC content can be evaluated as 5 wt.%. These results are consistent with the literature. In the study conducted by Li et al. (2023) [37], Ni-SiC was produced by electrodeposition method. It has been reported that I_{corr} decreases and R_p increases with increasing SiC content in composite coatings; this improvement is related to the SiC particles promoting grain refinement and reducing coating porosity.

The electrochemical impedance data were obtained in accordance with the equivalent circuit model (R_1 + Q_1/(R_2 + C_3/R_3)) (Table 5). Here, R_1 is the electrolyte resistance; Q_1 is the constant phase element representing the non-ideal double layer capacitance; R_2 and R_3 show the resistance components associated with charge transfer and barrier properties between the coating and the substrate; C_3 is the capacitance of the interface between substrate and coating, respectively. According to the Nyquist plots (Figure 7c), the uncoated sample exhibits the smallest semicircle diameter, and the lowest impedance components (R_2 = 2.718 Ω, R_3 = 287.9 Ω) were measured for the uncoated Inconel 600 sample, indicating direct electrolyte–metal contact without an effective protective film. After Ni-Al-Cr coating, an increase in impedance parameters (R_2 = 9.071 Ω, R_3 = 299.1 Ω) was observed, confirming the formation of a passive barrier layer that limits ion transport and improves corrosion resistance [38,39]. Garcia et al. (2003) [36] reported that SiC reinforcement enhances microstructural continuity in composite coatings, leading to an enlarged impedance radius and improved load transfer resistance. With increasing SiC content, a pronounced enhancement in impedance response is observed, reflecting improved coating compactness and passive layer stability. While the coatings containing 1 wt.% and 3 wt.% SiC showed noticeable improvements in R_2 and R_3 values, the 5 wt.% SiC-reinforced coating exhibited the highest R_2 value (1188 Ω), indicating the most effective charge transfer resistance and barrier performance among all samples. This behavior suggests that a higher SiC fraction contributes to a denser coating structure and a more resistive passive layer, effectively suppressing electrolyte penetration. According to Overall, the EIS analysis confirms that the Ni-Al-Cr coating containing 5 wt.% SiC provides the most effective corrosion protection, exhibiting the highest impedance response and the most stable passive film structure.

Table 5. EIS Nyquist fittings of equivalent circuit (R_1 + Q_1/(R_2 + C_3/R_3)) diagrams.

Sample	R_1 (Ω)	Q_1 ($10^{-3} \times F \times s^{(a-1)}$)	a	R_2 (Ω)	C_3 (F)	R_3 (Ω)
Uncoated (S1)	4.21	2.49	0.78	2.718	49.05×10^{-6}	287.9
Ni-Al-Cr (S2)	2.97	3.26	0.74	9.071	0.557×10^{-3}	299.1
Ni-Al-Cr/1%SiC (S3)	5.41	1.80	0.74	600.7	4.099×10^{-3}	0.758
Ni-Al-Cr/3%SiC (S4)	5.85	3.22	0.70	600.2	29.23×10^{-6}	686.1
Ni-Al-Cr/5%SiC (S5)	2.55	0.18	0.77	1188	54.56×10^{-6}	2.715

4. Conclusions

In this study, the microstructural, mechanical, and corrosion properties of Ni-Al-Cr coatings produced with 1%, 3%, and 5% SiC reinforcement on Inconel 600 substrates were comprehensively investigated.

- ✓ SiC reinforcement significantly increased the hardness of the coating. The coating containing 5% SiC had the highest hardness value. In coatings containing 1% and 3% SiC, a relative reduction in wear rate was achieved due to the uniform distribution of SiC particles within the matrix and the limitation of dislocation movement.
- ✓ The increased wear rate in the 5% SiC-reinforced coating was attributed to the formation of microcracks and increased brittle behavior due to the high SiC content.
- ✓ Corrosion of SiC-reinforced coatings exhibited increased corrosion resistance with the formation of a more stable passive film and an increase in the SiC ratio. This demonstrates that SiC improves corrosion resistance as well as providing mechanical strength to the coating structure.
- ✓ These results reveal that Ni–Al–Cr/SiC composite coatings have strong potential in industrial applications where high temperature, erosion, oxidation, and wear are critical. In conclusion, SiC-reinforced Ni-Al-Cr coatings, especially with 1–3% SiC content, provide superior hardness, wear resistance, and microstructural integrity, while 5% SiC reinforcement limits wear behavior. Hardness and corrosion resistance improved with increasing SiC content. Wear resistance decreased after 3% SiC reinforcement.
- ✓ Future studies could investigate the effects of different SiC or other ceramics (TiC, Nb_2C, etc.) on coating performance. This could involve testing composite coatings with different substrate materials and coating methods in a wider range of industrial applications. Thermal analyses could be performed to evaluate the long-term durability of the coatings at high temperatures.

Funding: This study was supported by Hakkari University Scientific Research Projects Coordination Unit. Project Number: FM24BAP10. The author would like to thank the Van Yuzuncu Yil University Science Application and Research Center and its staff for their support in material characterization.

Institutional Review Board Statement: Not applicable.

Informed Consent Statement: Not applicable.

Data Availability Statement: The data presented in this study are available on request from the corresponding author.

Conflicts of Interest: The author declares no conflicts of interest.

References

1. Sato, Y.S.; Arkom, P.; Kokawa, H.; Nelson, T.W.; Steel, R.J. Effect of microstructure on properties of friction stir welded Inconel Alloy 600. *Mater. Sci. Eng. A* **2008**, *477*, 250–258. [CrossRef]
2. Was, G.S. Grain-boundary chemistry and intergranular fracture in austenitic nickelbase alloys. A review. *Corrosion* **1990**, *46*, 319–330. [CrossRef]

3. Al-Rubaie, K.S.; Godefroid, L.B.; Lopes, J.A.M. Statistical modeling of fatigue crack growth rate in Inconel alloy 600. *Int. J. Fatigue* **2007**, *29*, 931–940. [CrossRef]
4. Kulka, M.; Dziarski, P.; Makuch, N.; Piasecki, A.; Miklaszewski, A. Microstructure and properties of laser-borided Inconel 600-alloy. *Appl. Surf. Sci.* **2013**, *284*, 757–771. [CrossRef]
5. Kumar, S.; Prasad, B.S.; Kain, V.; Reddy, J. Methods for making alloy 600 resistant to sensitization and intergranular corrosion. *Corros. Sci.* **2013**, *70*, 55–61. [CrossRef]
6. Huang, J.; Liu, S.; Yu, S.; An, L.; Yu, X.; Fan, D.; Yang, F. Cladding Inconel 625 on cast iron via bypass coupling micro-plasma arc welding. *J. Manuf. Process.* **2020**, *56*, 106–115. [CrossRef]
7. Sitek, R.; Sikorski, K.; Sobczak, J.; Wierzchoń, T. Structure and properties of the multilayers produced on Inconel 600 by the PACVD method with the participation of trimethylaluminum vapours. *Mater. Sci.-Pol.* **2008**, *26*, 767.
8. Makuch, N.; Kulka, M. Microstructural characterization and some mechanical properties of gas-borided Inconel 600-alloy. *Appl. Surf. Sci.* **2014**, *314*, 1007–1018. [CrossRef]
9. Rakhadilov, B.; Buitkenov, D.; Apsezhanova, A.; Kakimzhanov, D.; Nabioldina, A.; Magazov, N. Selection of Optimal Process Parameters for Arc Metallization. *Coatings* **2025**, *15*, 300. [CrossRef]
10. Ning, J.; Lan, Q.; Zhu, L.; Xu, L.; Yang, Z.; Xu, P.; Xin, B. Microstructure and mechanical properties of SiC-reinforced Inconel 718 composites fabricated by laser cladding. *Surf. Coat. Technol.* **2023**, *463*, 129514. [CrossRef]
11. Makuch, N.; Dziarski, P. The Importance of Laser Beam Power on the Microstructure and Wear Behavior of Al-WC Composite Layers Produced by Laser Surface Alloying. *Materials* **2025**, *18*, 1899. [CrossRef] [PubMed]
12. Ghadami, F.; Sohi, M.H.; Ghadami, S. Effect of TIG surface melting on structure and wear properties of air plasma-sprayed WC–Co coatings. *Surf. Coat. Technol.* **2015**, *261*, 108–113. [CrossRef]
13. Xie, X.M.; Liu, X.B.; He, B.M.; Zhang, F.Z.; Liang, J.X.; Liu, X.Y.; Zheng, J. Laser cladding Ni60-SiC/Ti_3SiC_2 self-lubricating composite coatings on IN718 alloy: Wear mechanisms and oxidation behaviors. *Wear* **2025**, *560*, 205611. [CrossRef]
14. Wang, T.; An, Y.; Sun, P.; Zhao, W.; Zhou, L.; Liu, X. Impact of different nanosized-WC contents on the microstructure and wear resistance of direct energy deposition Inconel 625/WC composites by circular beam oscillating laser. *Ceram. Int.* **2025**, *51*, 15557–15570. [CrossRef]
15. Calderón, J.A.; Henao, J.E.; Gómez, M.A. Erosion–corrosion resistance of Ni composite coatings with embedded SiC nanoparticles. *Electrochim. Acta* **2014**, *124*, 190–198. [CrossRef]
16. Medelien, V. The influence of B4C and SiC additions on the morphological, physical, chemical and corrosion properties of Ni coatings. *Surf. Coat. Technol.* **2002**, *154*, 104–111. [CrossRef]
17. Maurya, R.; Katiyar, P.K.; Yadav, P.C.; Rani, P. Influence of pulse frequency on microstructure, mechanical properties, and corrosion resistance of electrodeposited Ni-SiC composite coatings. *Mater. Today Commun.* **2024**, *40*, 109977. [CrossRef]
18. Hou, T.; Duan, H.; Zhang, G.; Yang, T.; Huang, C.; Zhan, S.; Jia, D. Tribocorrosion behavior and mechanism of Ni/SiC composite coating in multiple conditions. *Mater. Today Commun.* **2025**, *49*, 113966. [CrossRef]
19. *ASTM G59*; Standard Test Method for Conducting Potentiodynamic Polarization Resistance Measurements. ASTM International: West Conshohocken, PA, USA, 2014.
20. Kilic, M.; Imak, A.; Kirik, I. Surface modification of AISI 304 stainless steel with NiBSi-SiC composite by TIG method. *J. Mater. Eng. Perform.* **2021**, *30*, 1411–1419. [CrossRef]
21. Prabu, S.S.; Ramkumar, K.D.; Arivazhagan, N. Microstructural evolution and precipitation behavior in heat affected zone of Inconel 625 and AISI 904L dissimilar welds. In *IOP Conference Series: Materials Science and Engineering*; IOP Publishing: Bristol, UK, 2017; Volume 263, p. 062073.
22. Islak, S.; Eski, Ö.; Buytoz, S. Microstructure and wear properties of FeW SiC based composite coating produced with Tungsten inert gas (TIG) surfacing method. *Optoelectron. Adv. Mater.-Rapid Commun.* **2011**, *5*, 665–672.
23. Xu, J.; Gao, P.; Wang, W.; He, W.; Jiang, S.; Pan, X.; Liu, X. Study on optical and mechanical properties of SiC single-crystal substrate at high temperature. *J. Mater. Sci. Mater. Electron.* **2025**, *36*, 1–10. [CrossRef]
24. Liang, G.Y.; Zhu, C.; Wu, X.Y.; Wu, Y. The formation model of Ni–Cr oxides on NiCoCrAlY-sprayed coating. *Appl. Surf. Sci.* **2011**, *257*, 6468–6473. [CrossRef]
25. Gray, S.; Mphahlele, M.; Collins, D.M.; Jackson, C.; Hardy, M.C.; Taylor, M.P. Comparison of Performance of $NiCr_2O_4$ and Cr_2O_3 Formed on the Ni-Based Superalloy RR1000 Under Corrosive Conditions. *High Temp. Corros. Mater.* **2024**, *101*, 1091–1102. [CrossRef]
26. Suwarno, S.; Nugroho, D.N.; Yudanto, F.; Prawara, B. The Effect of SiC in NiCrBSi-SiC Composite Coating on the Microstructure, Hardness, and Oxidation Resistance. *J. Rekayasa Mesin* **2021**, *12*, 581–589. [CrossRef]
27. Yu, T.; Tang, H. Microstructure and high-temperature wear behavior of laser clad TaC-reinforced Ni-Al-Cr coating. *Appl. Surf. Sci.* **2022**, *592*, 153263. [CrossRef]
28. Wang, H.; Liu, H.; He, Y.; Ma, C.; Li, L. Ni-SiC composite coatings with good wear and corrosion resistance synthesized via ultrasonic electrodeposition. *J. Mater. Eng. Perform.* **2021**, *30*, 1535–1544. [CrossRef]

https://doi.org/10.3390/cryst16010049

29. Xu, Z.; Lu, Z.; Zhang, J.; Li, D.; Liu, J.; Lin, C. The friction and wear behaviours of Inconel 718 superalloys at elevated temperature. *Front. Mater.* **2021**, *8*, 794701. [CrossRef]
30. Feng, K.; Shao, T. The evolution mechanism of tribo-oxide layer during high temperature dry sliding wear for nickel-based superalloy. *Wear* **2021**, *476*, 203747. [CrossRef]
31. Wang, Y.; Jia, Z.; Ji, J.; Lu, W.; Liu, D. Tribo-oxidation mechanism of gradient nanostructured Inconel 625 alloy during high-temperature wear. *Wear* **2024**, *558*, 205581. [CrossRef]
32. Joshy, J.; Kuriachen, B. Influence of heat-treatment and cryo-treatment on high temperature wear performance of LPBF Inconel 718. *Wear* **2023**, *522*, 204681. [CrossRef]
33. Döleker, K.M.; Erdogan, A.; Yener, T.; Karaoglanlı, A.C.; Uzun, O.; Gök, M.S.; Zeytin, S. Enhancing the wear and oxidation behaviors of the Inconel 718 by low temperature aluminizing. *Surf. Coat. Technol.* **2021**, *412*, 127069. [CrossRef]
34. Zhang, Y.; Liu, Z.; Lv, Z.; Cao, J.; Tong, Y.; Sun, M.; Wang, X. Effect of SiC and TiC content on microstructure and wear behavior of Ni-based composite coating manufactured by laser cladding on Ti–6Al–4V. *Wear* **2024**, *552*, 205431. [CrossRef]
35. Li, J.; Cui, X.; Guan, Y.; Jin, G.; Zheng, W.; Liu, E.; Liu, A. Effect of SiC content on microstructural evolution and tribology properties of laser-clad TiC-reinforced Ti-Al-Si composite coatings. *Mater. Today Commun.* **2023**, *35*, 106019. [CrossRef]
36. Garcia, I.; Conde, A.; Langelaan, G.; Fransaer, J.; Celis, J.P. Improved corrosion resistance through microstructural modifications induced by codepositing SiC-particles with electrolytic nickel. *Corros. Sci.* **2003**, *45*, 1173–1189. [CrossRef]
37. Li, G.; Chen, Z.; Tan, Z.; Tian, R.; Zhao, Y.; Wang, L.; Liu, Y. Investigation on Microstructure and Properties of the Electrodeposited Ni-SiC Composite Coating. *Coatings* **2023**, *13*, 695. [CrossRef]
38. Topuz, M.; Teter, N. The Effect of Hydroxyapatite Fraction in Titanium—Hydroxyapatite Composite Coatings on Ti-6Al-4V Alloy with TIG Cladding. *Mater. Corros.* **2025**, *77*, 139–151. [CrossRef]
39. Topuz, M. In Vitro Corrosion and Bioactivity of Tungsten Inert Gas-Cladded AZ31-Zn Coatings on Ti-6Al-4V for Biomedical Applications. *J. Mater. Eng. Perform.* **2025**. [CrossRef]